Random matrix model for chiral and color-flavor locking condensates

T. Sano[1,2] and K. Yamazaki[1,2]

[1]*Institute of Physics, The University of Tokyo, Tokyo 153-8902, Japan*
[2]*Department of Physics, The University of Tokyo, Tokyo 113-0033, Japan*
(Received 6 September 2011; published 29 May 2012)

We study the phase diagram of a chiral random matrix model with three quark flavors at finite temperature and chemical potential, taking the chiral and diquark condensates as independent order parameters. Fixing the ratio of the coupling strengths in the quark-antiquark and quark-quark channels applying the Fierz transformation, we find that the color-flavor locked (CFL) phase is realized at large chemical potential, while the ordinary chirally broken phase appears in the region with small chemical potential. We investigate responses of the phases by changing small quark masses in the cases with three equal-mass flavors and with $2 + 1$ flavors. In the case with three equal-mass flavors, we find that the finite masses make the CFL phase transition line move to the higher-density region. In the case with $2 + 1$ flavors, we find the two-flavor color-superconducting phase at the medium-density region as a result of the finite asymmetry between the flavors, as well as the CFL phase at the higher-density region.

I. INTRODUCTION

Mapping of a QCD phase diagram at finite temperature and density [1–7] is one of the most challenging issues in the theoretical and experimental physics and is significant to the heavy-ion collision experiments and the structures of the neutron stars.

At finite temperature and zero or small baryon density, a number of investigations on QCD phase transitions are made both with the lattice QCD simulations [8] and with the model calculations [6]. Lattice QCD simulations suggest that the phase transition becomes a smooth cross-over in the realistic case with two light and one heavier quark flavors, and many model calculations are consistent with this result. At finite density, however, the situation is uncertain because lattice QCD simulations are still challenging at finite chemical potentials with low temperatures [9]. In such a region, it is important to employ models for qualitative and quantitative calculations on the phase diagram. Naively, a large baryon number density may cause overlaps of baryons, which invalidates a concept of confined colors in a baryon, resulting in deconfinement, which may be followed by chiral phase transition.

Furthermore, at asymptotically large density, the appearance of a color-superconducting (CSC) phase is also expected, where a weak coupling theory is applied and the Cooper instability of the Fermi sphere is inevitable [10,11]. The color-superconducting phases are characterized by the diquark condensates. One-gluon exchange interactions tell us that the color-antitriplet channel is attractive. Therefore, with the Pauli principle, condensates in the color- and flavor-antitriplet and spin-antisymmetric channel is expected. Such condensates can be expressed as [1]

$$s_{AA'} = \langle \bar{\psi}^c \gamma_5 \tau_A \lambda_{A'} \psi \rangle, \qquad (1)$$

where ψ is the quark field, and $\bar{\psi}^c = \psi^T C$ with C the charge conjugation operator. τ_A and λ_A, where $A = 2, 5,$ and 7, are the antisymmetric generators of $SU(N_f)$ flavor and $SU(N_c)$ color groups, respectively.

One of the most striking features in the CSC phases is the formation of the color-flavor locking (CFL) condensate [1]. At sufficiently high density, the finite current quark masses for up, down, and strange quark flavor are neglected so that the system can be treated as the chiral limit. In the CFL phase, which is characterized by $s_{AA'} = \Delta \delta_{AA'}$ with nonzero Δ, $SU(3)_L \otimes SU(3)_R \otimes SU(3)_c$ symmetry of the system breaks down to its subgroup of $SU(3)_{L+R+c}$. This breaking pattern is possible owing to the miraculous matching of the (effective) number of flavors $N_f = 3$ and the number of colors $N_c = 3$.

To investigate the QCD phase diagram at finite temperature and chemical potential, chiral random matrix (ChRM) models provide us with a qualitative way from a viewpoint of the symmetry [12,13]. In a conventional ChRM model, the Dirac operator is set as a random matrix, which has the same symmetry with QCD, and the partition function is defined as the average of the determinant of the Dirac operator over the matrix elements with the Gaussian distribution. The random distribution of the matrix elements mimics the complex dynamics of the gluon fields. The Gaussian model can be solved exactly in the thermodynamic limit. Although the model is constructed in such a simple way, the resulting phase diagram has a rich structure. In the chiral limit, the phase transition becomes second-order in the small chemical potential μ region, while it becomes first-order in the large μ region. First- and second-order phase transition lines are connected at the tricritical point (TCP). This result is consistent with Nambu–Jona-Lasinio (NJL).

The extension of the ChRM model to the case with the CSC phase has already been studied by Vanderheyden and

Jackson [16].[1] In their study, the Dirac matrix is extended to have the indices of color and spin explicitly with the real random matrices corresponding to real gluon fields in QCD. After the integration over the random matrices, the model produces the quark-quark interaction terms, which are responsible for the diquark condensates, as well as quark-antiquark interaction terms responsible for the chiral condensates. The resulting phase diagram has the diquark-condensed phase at large μ region, and the chirally broken phase at the small μ region, if the ratio of the quark-antiquark and the quark-quark coupling is taken so that the Dirac operator of the model has the same symmetry as that of QCD. Note that because the model in Ref. [16] contains two quark flavors, the CSC phase is the two-flavor color-superconducting (2SC) phase, where only two of three colors of fermions participate in the diquark pairing.

It is then natural to ask whether it is possible to extend the ChRM model to the case with three flavors, and whether the CFL phase can appear as the ground state in a high-density region. We answer "yes" to this question by constructing the ChRM model containing three flavors and colors and show a phase diagram with the chirally broken and the CFL phases. As a simple application of this model, we also focus on the response of the model by changing the quark masses. By setting the strange quark mass different from the other two quark flavors, we observe that the 2SC phase appears on the phase diagram at the moderate values of the chemical potential, as well as the CFL phase in the larger chemical potential region.

This paper is organized as follows. We introduce an extended ChRM model with chiral and CFL condensations in Sec. II and derive its effective potential in Sec. III. The model phase diagrams are presented and discussed in the case with three equal-mass flavors and $2 + 1$ flavors in Secs. IV and V, respectively. Section VI is devoted to a summary and discussion.

II. RANDOM MATRIX MODEL WITH CHIRAL AND DIQUARK CONDENSATIONS

In this section, we introduce a chiral random matrix model which mimics QCD partition function with three quark flavors, extending the two-flavor case in Ref. [16]. We denote three quark masses by m_f with $f =$ u, d, and s.

Keeping in mind the (extended) Banks-Casher relations, which relate Dirac soft modes not only with the chiral condensates [19], but also with the diquark condensates [20], we consider the truncated Dirac matrix D in low-lying quark excitation, or zero-mode space. We assume D can be separated as $D = R + C$, where R is a random part, which represents the complex gluon dynamics, and C the nonrandom, deterministic part, which is responsible for the matter effects.

For simplicity, we first set the matter effects turned off, i.e. $C = 0$, and focus on the random matrix R. In this case, the truncated Dirac matrix should have the symmetries of the Dirac operator in the vacuum, the chiral symmetry, $\{\gamma_5, R\} = 0$, and the anti-Hermiticity, $R^\dagger = -R$. Within these restrictions, the Dirac matrix generally has nonzero matrix elements only in the off-diagonal blocks

$$R = \begin{pmatrix} 0 & iW \\ iW^\dagger & 0 \end{pmatrix}, \quad (2)$$

in the chiral representation, $\gamma_5 = \mathrm{diag}(+1, -1)$, where W is a complex matrix.[2] In the conventional ChRM models [12], W is taken to be a general complex matrix whose elements are independently distributed according to the Gaussian distribution.

To consider the diquark condensations, however, it is crucial to treat the color and spin indices explicitly. Following the construction in Ref. [16], we express W as a direct product of the spin, color, and zero-mode matrices, whose total dimension is $2 \times N_c \times N$, where 2 is the size of the spin space, N_c the color space, and N the zero-mode space. We adopt the form of W as

$$W = A^{\nu a}(\sigma_\nu \otimes \lambda_a), \quad (3)$$

where $\sigma_\nu = (1, -i\sigma_i)$ with σ_i as the Pauli matrix, λ_a is a generator of $SU(N_c)$, and $A^{\nu a}$ is a $N \times N$ random matrix. Since the random matrix $A^{\nu a}$ corresponds to the gauge field in QCD, we choose $A^{\nu a}$ to be a real matrix.

The matter effects are introduced as the nonrandom external fields in the Dirac operator. A simple way [13] is to add a constant matrix C to the random matrix (2) with

$$C = \begin{pmatrix} 0 & \omega \\ \omega & 0 \end{pmatrix} = \omega \otimes \gamma_0, \quad (4)$$

where the $2 \times N_c \times N$-dimensional matrix ω is defined as

$$\omega = \begin{pmatrix} (\mu + iT)\mathbf{1}_{N/2} \otimes \mathbf{1}_{\mathrm{spin}} \otimes \mathbf{1}_{N_c} & 0 \\ 0 & (\mu - iT)\mathbf{1}_{N/2} \otimes \mathbf{1}_{\mathrm{spin}} \otimes \mathbf{1}_{N_c} \end{pmatrix}. \quad (5)$$

T and μ are an effective temperature and quark chemical potential, respectively. $\mathbf{1}_{\mathrm{spin}}$ denotes 2×2 identity matrix in the spin space. A total Dirac matrix, $D = R + C$, also has chiral symmetry, $\{D, \gamma_5\} = 0$, but not anti-Hermiticity, $D^\dagger \neq -D$ if $\mu \neq 0$. Two relative signs between T and μ correspond to the two lowest Matsubara frequencies, $\pm \pi T$. The inclusion of two signs reproduces the invariance

---

[1]Also, there are studies on the diquark condensates with $N_c = 2$ using ChRM models [17,18].

[2]One can take W generally to be an $N_+ \times N_-$ rectangular matrix. In this case, the Dirac matrix has $|\nu| = |N_+ - N_-|$ exact zero eigenvalues, which represents the index theorem with the background gauge field having the topological charge ν. Exploiting this fact, we can introduce the effect of the axial anomaly in the ChRM models [21,22]. In this study, however, we always take W to be square, and the anomaly effect is neglected. See the discussion in Sec. VI.

of the partition function under the charge conjugation transformation, $\mu \to -\mu$.

Using the Dirac matrix D, the ChRM model partition function is defined as

$$Z = \int [dA] \prod_{f=1}^{N_f} \det(D + m_f) e^{-2N\Sigma^2 \sum_{a,\nu,i,j} (A_{ij}^{\nu a})^2}, \quad (6)$$

where the integral is defined over real elements of random matrices $A^{\nu a}$ with the Gaussian weight. The parameter Σ, which fixes variance of the Gaussian distribution, gives a scale to the model. Generally, Σ may change for each a and ν, but by ensuring the color and Lorentz symmetry, their values should be equal.

Before solving the model, we make two remarks on the treatment of the ChRM model comparing to that in Ref. [16]. First, in Ref. [16], the authors examine not only the form of the random Dirac operator (2), but also the case where the Dirac operator breaks the symmetry which QCD Lagrangian holds. In such general cases, the random matrix R is taken as

$$(R)_{\alpha\beta} = \sum_{Ca} X_{\alpha\beta}^{Ca} (\Gamma_C)_{\alpha\beta} \otimes \lambda_a, \quad (7)$$

where the chiral indices α, β = R, L, $X_{\alpha\beta}^{Ca}$ is a random matrix, and Γ_C is the independent gamma matrix in four dimensions, $C = 1, \ldots 16$. A set of Γ_c can be separated into the subsets forming a Lorentz scalar, pseudoscalar, vector, axial-vector, and tensor. In Eqs. (2) and (3), we have chosen $X_{\alpha\beta}^{Ca}$ to be nonzero only for the vector content of the gamma matrices. This is a natural choice because we consider that the random matrices model the gluon fields, which form a Lorentz vector. Indeed, nonzero components for the scalar, pseudoscalar, and tensor break the chiral symmetry explicitly, and that for the axial-vector does the anti-Hermiticity. If such non-QCD-like random matrices are allowed, one can vary the ratio of the coefficients of the quark-antiquark and the quark-quark interaction channels, which is denoted as B/A in the next section. The evolution of the phase diagram with B/A changed was completely investigated in Ref. [16] for the case with two flavors. In our study, however, we only focus on the case for which the model has the same type of interaction as QCD, because the condition fixes the topology of the phase diagram without ambiguity, and we can solely concentrate on the response of the phase diagram by changing the quark masses.

Second, the scheme of the temperature dependence is different from that in Ref. [16]. We use the matter-effect matrix proportional to the identity in the flavor space, while, in Ref. [16], the sign of the temperature T is antisymmetric in the space of two flavors. As a result of this difference, our model cannot be reduced to the model in Ref. [16] in the two-flavor limit. Further discussion will be

given by comparing the effective potentials in the later section.

Finally, note that the partition function (6) has $SU(N_C)_c \otimes SU(N_f)_L \otimes SU(N_f)_L$ global symmetry, but not local gauge symmetry. To be exact, it is then appropriate to call the diquark-condensed phase a Bose-Einstein condensed state, not a BCS state. In the remaining part of this paper, we use the word "diquark condensates" to indicate such condensates, but discuss them compared to the BCS states expected in QCD at finite density.

III. THE EFFECTIVE POTENTIAL

In this section, we derive the effective potential of the ChRM model defined in Eq. (6). The derivation is almost parallel to that in Ref. [16]. We present the derivation in three steps and then make a few remarks.

A. Gaussian integral

The first step is to integrate out the Gaussian integral variables $A_{ij}^{a\mu}$. For this purpose, we first express the determinant in the partition function (6) in the form with the fermion integrals:

$$\prod_{f=1}^{N_f} \det(D + m_f)$$

$$= \int [d\psi^\dagger][d\psi] \exp\left[-\sum_f \bar\psi^f (D + m_f) \psi^f \right]$$

$$= \int [d\psi^\dagger][d\psi] \exp\left[-i J_{a\nu}^{ij} A_{ij}^{a\nu} - \sum_f \bar\psi^f (C + m_f) \psi^f \right], \quad (8)$$

where $\psi^f = (\psi_R^f, \psi_L^f)^T$ and $\bar\psi^f = (\psi_L^{f\dagger}, \psi_R^{f\dagger})$ are $4 \times N_c \times N$ Grassmann vectors, and

$$J_{a\nu}^{ij} = \sum_f (\psi_{Li}^{f\dagger} \sigma_\nu \lambda_a \psi_{Lj}^f + \psi_{Rj}^{f\dagger} \sigma_\nu^\dagger \lambda_a \psi_{Ri}^f) \quad (9)$$

is a fermion bilinear.

Applying the Gaussian integral formula up to the constant, $\int dx e^{-\alpha x^2 + \beta x} = \exp(\beta^2/(4\alpha))$, to the $A_{a\nu}^{ij}$ integral separately for each indices i, j, a, and ν, we obtain analytically

$$\int [dA] e^{-i J_{a\nu}^{ij} A_{ij}^{a\nu}} e^{-2N\Sigma^2 (A_{ij}^{a\nu})^2} = \exp\left[-\frac{1}{8N\Sigma^2} (J_{a\nu}^{ij})^2 \right], \quad (10)$$

where the summations over i, j, a, and ν should be understood on the right-hand side.

B. Fierz transformation

In this step, we expand the square of the fermion bilinear $(J_{a\nu}^{ij})^2$ and realign the four-point vertices by applying the Fierz transformation formula. The square of $J_{a\nu}^{ij}$ is expanded as

$$(J_{a\nu}^{ij})^2 = 2\psi_{Ri}^{f\dagger}\sigma_\nu^\dagger\lambda_a\psi_{Rj}^f\psi_{Lj}^{g\dagger}\sigma_\nu\lambda_a\psi_{Li}^g$$
$$+ \psi_{Li}^{f\dagger}\sigma_\nu\lambda_a\psi_{Lj}^f\psi_{Li}^{g\dagger}\sigma_\nu\lambda_a\psi_{Lj}^g$$
$$+ \psi_{Ri}^{f\dagger}\sigma_\nu^\dagger\lambda_a\psi_{Rj}^f\psi_{Ri}^{g\dagger}\sigma_\nu^\dagger\lambda_a\psi_{Rj}^g. \quad (11)$$

The first term represents the quark-antiquark interactions, and the other terms the quark-quark interactions. The former is responsible for the formation of the chiral condensates and the latter for the diquark condensates.

Using Fierz transformations, these four-fermion terms are rearranged so that in each fermion bilinear term, zero-mode indices i and j are contracted. At this point, we assume that the chiral condensates are formed only in the color-singlet, scalar channels and that the diquark condensates are formed only in the spin-antisymmetric, flavor- and color-antitriplet, scalar channels. With these assumptions, relevant interaction terms are drastically reduced and shown explicitly as[3]

$$\psi_{Ri}^{f\dagger}\sigma_\mu^\dagger\lambda_a\psi_{Rj}^f\psi_{Lj}^{g\dagger}\sigma_\mu\lambda_a\psi_{Li}^g = -\frac{2(N_c^2-1)}{N_c^2}\psi_R^{f\dagger}\psi_L^g\psi_L^{g\dagger}\psi_R^f$$
$$+ \dots \quad (12)$$

for quark-antiquark channels and

$$\psi_{Li}^{f\dagger}\sigma_\mu\lambda_a\psi_{Lj}^f\psi_{Li}^{g\dagger}\sigma_\mu\lambda_a\psi_{Lj}^g$$
$$= -\frac{N_c+1}{2N_c}\psi_L^\dagger\tau_A\lambda_{A'}\psi_L^c\psi_L^{c\dagger}\tau_A\lambda_{A'}\psi_L + \dots \quad (13)$$

for quark-quark channels, with the same except L → R, where the charge conjugation fields are defined as $\psi^c \equiv C\bar\psi^T = (\psi_L^c, \psi_R^c)^T$ and $\bar\psi^c \equiv \psi^T C = (\psi_R^{c\dagger}, \psi_L^{c\dagger})$. The dots denote the terms irrelevant to the formation of the condensates we focus on.

Neglecting the irrelevant terms, we finally obtain the simple form of four-point interaction as

$$(J_{a\nu}^{ij})^2 = -2G_\chi\psi_R^{f\dagger}\psi_L^g\psi_L^{g\dagger}\psi_R^f$$
$$- G_\Delta\psi_L^\dagger\tau_A\lambda_{A'}\psi_L^c\psi_L^{c\dagger}\tau_A\lambda_{A'}\psi_L + \{\text{L}\to\text{R}\}, \quad (14)$$

where we have defined coefficients $G_\chi = \frac{2(N_c^2-1)}{N_c^2}$ and $G_\Delta = \frac{N_c+1}{2N_c}$.

C. Bosonization

We apply the Hubbard-Stratonovich transformation formula, $e^{\beta_1\beta_2\alpha} = \int dz e^{-\alpha|z|^2+\beta_1 z+\beta_2 z^*}$, to the rearranged four-point interaction (14). For simplicity, we make further, but moderate assumptions in the formation of the chiral and diquark condensates. For chiral condensates, we assume that only the flavor-singlet condensates are formed, and for diquark condensates, that only the color-flavor-locked condensates are formed, i.e., $s_{AA'} = \langle\psi_L^{c\dagger}\tau_A\lambda_{A'}\psi_L\rangle \propto \delta_{AA'}$. These assumptions allow us to bosonize the fermion vertex (10) as

$$\exp\left[-\frac{1}{8N\Sigma^2}(J_{a\nu}^{ij})^2\right] = \int[d\phi][d\Delta]\exp\left(-\frac{N\Sigma^2}{2G_\chi}2|\phi_f|^2 - \frac{N\Sigma^2}{2G_\Delta}(|\Delta_A^L|^2 + |\Delta_A^R|^2)\right)$$

$$\times\exp\left[-(\phi_f^*\psi_R^{f\dagger}\psi_L^f + \psi_L^{f\dagger}\psi_R^f\phi_f) - \frac{1}{2}(\Delta_A^{L*}\psi_L^{c\dagger}\tau_A\lambda_A\psi_L + \psi_L^\dagger\tau_A\lambda_A\psi_L^c\Delta_A^L) - \{\text{L}\to\text{R}\}\right]$$

$$= \int[d\phi][d\Delta]\exp\left(-\frac{N\Sigma^2}{2G_\chi}2|\phi_f|^2 - \frac{N\Sigma^2}{2G_\Delta}(|\Delta_A^L|^2 + |\Delta_A^R|^2)\right)\exp[-\Psi_L^\dagger S\Psi_R - \Psi_R^\dagger S^\dagger\Psi_L], \quad (15)$$

where the measure $[d\phi][d\Delta] = \prod_{f=u,d,s}\prod_{A=2,5,7} \times d\phi_f d\Delta_A^L d\Delta_A^R$. We have defined the Nambu-Gorkov spinors by

$$\Psi = \frac{1}{\sqrt{2}}\begin{pmatrix}\Psi_R \\ \Psi_L\end{pmatrix} = \frac{1}{\sqrt{2}}\begin{pmatrix}\psi_R \\ \psi_L^c \\ \psi_L \\ \psi_R^c\end{pmatrix} \quad (16)$$

and

$$\bar\Psi = \frac{1}{\sqrt{2}}(\Psi_L^\dagger, \Psi_R^\dagger) = \frac{1}{\sqrt{2}}(\psi_L^\dagger, \psi_R^{c\dagger}, \psi_R^\dagger, \psi_L^{c\dagger}), \quad (17)$$

and the $2\times N_C\times N_f(=18)$-dimensional order parameter matrix S by

$$S = \begin{pmatrix}\hat\phi\mathbf{1}_{N_c} & \Delta_A^L\tau_A\lambda_A \\ \Delta_A^{R*}\tau_A\lambda_A & \hat\phi\mathbf{1}_{N_c}\end{pmatrix}, \quad (18)$$

where $\hat\phi = \text{diag}(\phi_u, \phi_d, \phi_s)$ is a matrix in the flavor space.

By representing the mass and matter-effect terms in the Nambu-Gorkov basis, we obtain the partition function as

$$Z = \int[d\psi^\dagger][d\psi][d\phi][d\Delta]$$

$$\times\exp\left(-\frac{N\Sigma^2}{2G_\chi}2|\phi_f|^2 - \frac{N\Sigma^2}{2G_\Delta}(|\Delta_A^L|^2 + |\Delta_A^R|^2)\right)$$

$$\times\exp\left[-\bar\Psi\begin{pmatrix}S+\mathcal{M} & \tilde{C} \\ \tilde{C} & S^\dagger+\mathcal{M}^\dagger\end{pmatrix}\Psi\right], \quad (19)$$

where $\tilde{C} = \text{diag}(\omega, -\omega)$ and $\mathcal{M}$ is the extended mass matrix

---

[3]For the Fierz transformation formulae, see, for example, Ref. [7].

$$\mathcal{M} = \begin{pmatrix} \hat{m}\mathbf{1}_{N_c} & -\eta_A \tau_A \lambda_A \\ \eta_A^* \tau_A \lambda_A & \hat{m}\mathbf{1}_{N_c} \end{pmatrix} \qquad (20)$$

with mass matrix $\hat{m} = \mathrm{diag}(m_u, m_d, m_s)$ in the flavor space. We have introduced the external field η_A, which should be zero in the end of the calculation. It is useful to clarify the meaning of the order parameters.

Finally, the evaluation of the fermion integral is straightforward, which yields

$$Z = \int [d\phi][d\Delta] \exp\left(-\frac{N\Sigma^2}{2G_\chi} 2|\phi_f|^2 - \frac{N\Sigma^2}{2G_\Delta}(|\Delta_A^L|^2 + |\Delta_A^R|^2)\right)$$

$$\times \left[\det^{N/2}\begin{pmatrix} S + \mathcal{M} & \tilde{z} \\ \tilde{z} & S^\dagger + \mathcal{M}^\dagger \end{pmatrix} \right.$$

$$\times \left. \det^{N/2}\begin{pmatrix} S + \mathcal{M} & \tilde{z}^* \\ \tilde{z}^* & S^\dagger + \mathcal{M}^\dagger \end{pmatrix} \right]^{1/2}$$

$$= \int [d\phi][d\Delta] e^{-2NN_f N_c \Omega(\phi, \Delta; m, T, \mu)}, \qquad (21)$$

where $\tilde{z} = \mathrm{diag}(z, -z)$ with $z \equiv (\mu + iT)\mathbf{1}_{N_f}\mathbf{1}_{N_C}$. The square root over the determinant is given because the number of the fermion measures is a half of that of the Nambu-Gorkov basis. We have defined the effective potential Ω as the function of the order parameters. In the thermodynamic limit, $N \to \infty$, the ground state of the model is determined by the set of the order parameters which minimizes the effective potential.

For the ground-state solutions, we make a few *Ansätze* for the order parameters. First, we set ϕ_f to be real, $\phi_f^* = \phi_f$. Second, we also set Δ_A^L and Δ_A^R to be real and $-\Delta_A^L = \Delta_A^R \equiv \Delta_A$. Both assumptions are consistent for the formation of the scalar and parity-positive condensates in the ground state, which are favored by the finite quark mass term and the real η_A. Then, the effective potential is a function of six order parameters, ϕ_f with $f = u, d$, and s and Δ_A with $A = 2, 5$, and 7. Using these assumptions, the effective potential Ω becomes

$$\Omega = \frac{B}{3}\phi_f^2 + \frac{A}{3}\Delta_A^2 - \frac{1}{8N_c N_f}[\mathrm{lndet}(S + \mathcal{M} + z)$$

$$+ \mathrm{lndet}(S^\dagger + \mathcal{M}^\dagger - z) + \mathrm{lndet}(S + \mathcal{M} + z^*)$$

$$+ \mathrm{lndet}(S^\dagger + \mathcal{M}^\dagger - z^*)], \qquad (22)$$

where $A = 3\Sigma^2/(2N_c N_f G_\Delta)$ and $B = 3\Sigma^2/(2N_c N_f G_\chi)$ are defined. Note that we have omitted the 2-dimensional identity matrix multiplied by z for simplicity. In the thermodynamic limit, we can obtain the ground state by solving the six gap equations, $\partial\Omega/\partial\phi_f = 0$ and $\partial\Omega/\partial\Delta_A = 0$, simultaneously.

D. Remarks

To relate the order parameters in the ChRM model with the expectation values of the fermion bilinears in the microscopic theory, we use the external field derivatives as

$$\langle \bar{\psi}_f \psi_f \rangle \equiv -\lim_{N\to\infty} \frac{1}{2NN_c N_f} \frac{\partial \ln Z}{\partial m_f} = \frac{2B}{3}\phi_f, \qquad (23)$$

$$s_{AA} = \langle \bar{\psi}^c \tau_A \lambda_A \gamma_5 \psi \rangle \equiv -\lim_{N\to\infty} \frac{1}{2NN_c N_f} \frac{\partial \ln Z}{\partial \eta_A} = \frac{2A}{3}\Delta_A. \qquad (24)$$

The order parameters ϕ_f and Δ_A are proportional to the chiral and the diquark condensates, respectively, and then we simply use the values of ϕ_f and Δ_A to distinguish each phase.

Note that, in the partition function, the parameter Σ can be absorbed by rescaling the order parameters, as well as the parameters T, μ, m_f, and η_A. Therefore, in the chiral limit $m_f = 0$ (together with $\eta_A = 0$), a change of Σ affects only on the scale of the phase diagram, and the global structure of the phase diagram is invariant. In fact, the parameter which can change the structure of the phase diagram is B/A, which is independent of Σ. In our treatment, the ratio is fixed by the Fierz coefficients and is obtained as $B/A = 3/8$ with $N_c = 3$. In Ref. [16], various structures of the phase diagrams have been found with B/A changed.

IV. THREE EQUAL-MASS FLAVORS

We first examine the ground state in the case with the exact flavor SU(3) symmetry. For this purpose, we set $m_u = m_d = m_s = m$. Assuming that the flavor symmetry is not broken spontaneously, we can set the order parameters as $\phi_u = \phi_d = \phi_s \equiv \phi$ and $\Delta_2 = \Delta_5 = \Delta_7 \equiv \Delta$.

The effective potential is simplified to the function of the two order parameters,

$$\Omega = A\Delta^2 + B\phi^2 - \frac{1}{72}\sum_{\pm} \ln[(\sigma \pm z)^2 + \Delta^2]^8$$

$$\times [(\sigma \pm z)^2 + (2\Delta)^2] + \mathrm{c.c.}, \qquad (25)$$

where $\sigma = \phi + m$, and we have set $\eta_A = 0$. The terms under the logarithm may correspond to eight degenerated quasiparticles with mass $m + \phi + \Delta$ and one quasiparticle with mass $m + \phi + 2\Delta$ [1]. Combining two gap equations, $\partial\Omega/\partial\phi = 0$ and $\partial\Omega/\partial\Delta = 0$, we can determine a ground-state solution for given T, μ, and m.

It is easy to find that $\Delta = 0$ is always a solution of the gap equation, since Δ appears as Δ^2 in the effective potential. Moreover, if $m = 0$, $\phi = 0$ is also a trivial solution for any T and μ. Then, in the chiral limit, there are generally four types of the solutions: (i) $\phi = 0$, $\Delta = 0$, (ii) $\phi \neq 0$, $\Delta = 0$, (iii) $\phi = 0$, $\Delta \neq 0$, and (iv) $\phi \neq 0$, $\Delta \neq 0$. When $m \neq 0$, the solution $\phi = 0$ no longer exists and is replaced by a small value proportional to m.

Let us first consider solutions with $\Delta = 0$. When $\Delta = 0$, the effective potential (25) becomes identical with that analyzed in Ref. [13],

$$\Omega = \frac{G^2}{2}\phi^2 - \frac{1}{4}\ln(\sigma^2 - z^2) - \frac{1}{4}\ln(\sigma^2 - z^{*2}), \quad (26)$$

where $G^2 = 2B$ is defined. Therefore, the phase diagram described by the effective potential (25) at $\Delta = 0$ is the same as in Ref. [13]. Several points on the phase structure with the effective potential (26) are summarized: When $m = 0$, we find a second-order phase boundary in the large T and small μ region, and a first-order phase boundary in the small T and large μ region. Two lines are connected at the TCP, $(T_3, \mu_3) = \left(\frac{1}{2}\sqrt{\sqrt{2}+1}G^{-1}, \frac{1}{2} \times \sqrt{\sqrt{2}-1}G^{-1}\right) = (0.776G^{-1}, 0.322G^{-1})$. The transition temperature at $\mu = 0$ is obtained as $T_0 = G^{-1}$, while the transition chemical potential at $T = 0$ is $\mu_0 = 0.528G^{-1}$. We use these two values of T_0 and μ_0 for a normalization of T and μ in the presentation of the phase diagram to remove the Σ dependence as possible. If finite m is introduced, the second-order phase transition line becomes a smooth crossover, while the first-order line remains. The TCP also becomes the critical point.

We next consider the solutions with $\phi = 0$. By setting $\phi = 0$ and $m = 0$, the effective potential becomes

$$\Omega = A\Delta^2 - \frac{1}{4}\left[\frac{8}{9}\ln(\Delta^2 + z^2) + \frac{1}{9}\ln(4\Delta^2 + z^2)\right] + \text{c.c.} \quad (27)$$

The gap equation for a nontrivial solution $\Delta \neq 0$ is obtained as

$$A - \frac{1}{4}\left[\frac{8}{9}\frac{1}{\Delta^2 + z^2} + \frac{1}{9}\frac{4}{4\Delta^2 + z^2}\right] + \text{c.c.} = 0. \quad (28)$$

For a large T and/or μ, this equation does not have a real solution of Δ, which indicates that at some values of T and μ, its solution coalesces to the trivial solution $\Delta = 0$, where the system reaches a second-order phase transition.

It is easy to find a curve of the phase transition by setting $\Delta = 0$ in Eq. (28):

$$\frac{\mu^2 - T^2}{(\mu^2 + T^2)^2} = \frac{2A}{3}. \quad (29)$$

The true phase structure should be, of course, determined by comparing the effective potential for all solutions of the gap equations, and the second-order phase transition line (29) may be replaced by other phase structures.

To investigate the whole phase diagram, we have to numerically compare the effective potentials for all possible solutions. The result is presented in Fig. 1 for the case with $m = 0$ (left panel) and with $m \neq 0$ (right panel).

In the chiral limit, we find a $\Delta = 0$ solution becomes the ground state for a small chemical potential $\mu/\mu_0 \lesssim 0.95$. In this region, the phase diagram is the same as that investigated in Ref. [13]: There is the second-order phase transition line between the T axis and the TCP and the first-order line from TCP to the large μ region.

When a chemical potential exceeds a critical value, however, we find a first-order phase transition to the CFL phase at a small temperature. In this phase, the chiral order parameter ϕ becomes zero. We stress that the phase transition to the CFL phase in the ChRM model is remarkable because in the construction of the ChRM model, the ratio of the couplings between the quark-antiquark and the quark-quark channels is given by the symmetry consistent with QCD, not tuned so that the phase transition can be reproduced.

Unfortunately, on the other hand, the CFL condensate Δ continuously goes to zero not only as T is increased, but also as μ is. In QCD, the second-order phase transition at a large μ is not expected, since the Cooper instability remains even if the attractive interaction is infinitely small. This unphysical phase transition may be explained by the absence of the Fermi surface in the ChRM model, which is regarded as a model without the spatial dimension. We consider that, at such a region, the model reaches a limitation. Similar structures are found in the ChRM models for two-color QCD with the diquark baryon condensates
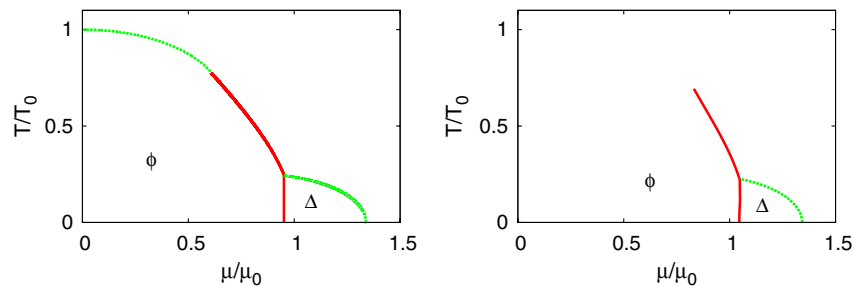

FIG. 1 (color online).   The phase diagrams with three equal-mass flavors. The left (right) panel shows the case with $m = 0$ ($\Sigma m = 0.1$). The solid lines denote the first-order phase transitions, and the dotted lines the second-order phase transitions. The largest order parameters in each phases are shown by its letter. T_0 (μ_0) is defined as the chiral phase transition temperature (chemical potential) on the T (μ) axis in the chiral limit when $\Delta = 0$.

[17,18], as well as in the study on the 2SC phase in the ChRM model [16].

When $m \neq 0$ (the right panel of Fig. 1), we find qualitative and quantitative changes from the case with $m = 0$. Because of the nonzero m, ϕ has a small value even in the symmetric and the CFL phases. The second-order chiral phase transition line is washed out to become a crossover, and then the TCP becomes a critical point. Note that the second-order phase transition line for Δ remains. The first-order chiral phase transition line is pulled up in the larger T and μ directions. The phase transition line between the chirally-broken phase and the CFL phase also shifts to the larger μ region. Although the second-order CFL phase transition line moves to extend the CFL phase, the CFL phase shrinks in total.

V. 2 + 1 FLAVORS

We next concentrate on the response of the model to the asymmetry between the light up and down (ud) quark flavors and the mid-light strange quark flavor. In order to see this effect, we set the quark masses as $m_u = m_d = m$ and $m_s \neq m$. We assume that the flavor symmetry is not broken further spontaneously and set the order parameters as $\phi_u = \phi_d = \phi$ and $\Delta_5 = \Delta_7 = \Delta_s$. We also write $\Delta_2 = \Delta$ for convenience. Because of the asymmetry between the ud and strange quarks, the typical symmetry in the CFL phase $SU_{c+L+R}(3)$ is not realized. Nevertheless, we call the phase with $\Delta \neq 0$ and $\Delta_s \neq 0$ the CFL phase. Also, the phase with $\Delta \neq 0$ and $\Delta_s = 0$ is defined as the 2SC phase.

Under the parametrization, the effective potential becomes the function of the four order parameters as

$$\Omega = \frac{A}{3}(\Delta^2 + 2\Delta_s) + \frac{B}{3}(2\phi^2 + \phi_s) - \frac{1}{72}\sum_{\pm}\ln[\{(\sigma \pm z)^2 + \Delta^2\}^3$$

$$\times \{(\sigma \pm z)(\sigma_s \pm z) + \Delta_s^2\}^4\{(\sigma_s \pm z)^2((\sigma \pm z)^2 + \Delta^2)$$

$$+ 4\Delta_s^2((\sigma \pm z)(\sigma_s \pm z) + \Delta_s^2)\}] + \text{c.c.}, \quad (30)$$

where $\sigma = \phi + m$, $\sigma_s = \phi_s + m_s$, and we set $\eta_A = 0$. For the general case with $\phi \neq \phi_s$ and $\Delta \neq \Delta_s$, the determinant part under the logarithm becomes complicated. By setting $m_s = m$, $\phi_s = \phi$, and $\Delta_s = \Delta$, we recover the effective potential in the three equal-mass limit (25). Another interesting limit is the 2SC phase, where $\Delta_s = 0$, in which the effective potential is separated to the ud quark sector and the strange quark sector as

$$\Omega = \Omega_{ud}(\phi, \Delta) + \Omega_s(\phi_s), \quad (31)$$

where

$$\Omega_{ud}(\phi, \Delta) = \frac{A}{3}\Delta^2 + \frac{2B}{3}\phi^2 - \frac{1}{72}\sum_{\pm}[4\ln((\sigma \pm z)^2 + \Delta^2)$$

$$+ 2\ln(\sigma \pm z)^2] + \text{c.c.} \quad (32)$$

and

$$\Omega_s(\phi_s) = \frac{B}{3}\phi_s^2 - \frac{1}{72}\sum_{\pm}\ln(\sigma_s \pm z)^6 + \text{c.c.} \quad (33)$$

The effective potential for the strange quark flavor (33) is equivalent to the one of the conventional ChRM model without diquark condensates [13], whose phase structure is summarized in Sec. IV.

The effective potential (32) can be compared to the one in Ref. [16], where two light quark flavors are introduced, and the strange quark degree of freedom is neglected. We first point out that the ratio of the coefficients of the quadratic terms of the order parameters, which can be read from Eq. (32) as $(2B/3)/(A/3) = 2B/A = 3/4$ since $B/A = 3/8$, is equal to that appearing in the model in Ref. [16]. The reproduction of $3/4$ is important since the phase structure is sensitive to this ratio.

Interestingly, however, these two effective potentials are not completely equivalent and match only if $T = 0$ or $\Delta = 0$. This is because we use the different temperature scheme, or the matter effect matrix (4), from that used in Ref. [16]. In the scheme used in Ref. [16], the effective temperature is introduced with opposite signs for two flavors.[4] On the other hand, in the scheme we used here, the temperature is introduced proportionally to the identity in the flavor space. The relation of these schemes is discussed in detail in Ref. [23].

By considering the microscopic theory, a reason of the choice of the flavor-antisymmetric scheme can be explained as follows [23]: To make the flavor-antisymmetric quark pair condensate be independent of the imaginary time τ, only the terms of two quark fields with the opposite signs of the Matsubara frequencies should be nonzero in the Fourier summation over the Matsubara frequencies. This indicates that the temperature term, or the lowest Matsubara frequencies, should have the opposite signs for different flavors because, in the diquark pairing, two quarks have different flavors in our treatment.

Nevertheless, we use the flavor-symmetric scheme in this paper because of the following reasons. First, if we construct the ChRM model relying only on the symmetry, we cannot find a scheme which has to be adopted. Both treatments are consistent with the QCD symmetry, the anti-Hermiticity at $\mu = 0$, and the chiral symmetry for all T and μ of the Dirac operator. Second, because we treat the ChRM model in the case with three flavors, in order to adopt the flavor-antisymmetric scheme, we have to concern contributions from three combinations of the three flavors. This might make the effective potential more complicated, and we try to make the model as simple as possible. Indeed, the resulting phase diagram, which will be shown below, is qualitatively equivalent to the model with the flavor-antisymmetric scheme at $\Delta_s = 0$. In other words, they

---

[4]Superficially, it seems to break the flavor symmetry, but, indeed, the symmetry is held if the chemical potentials for two flavors are equal [23].
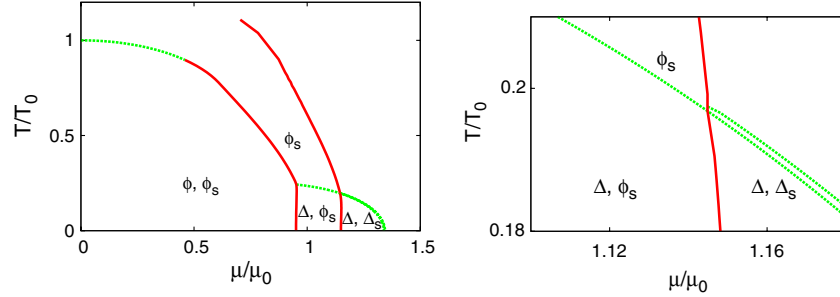
FIG. 2 (color online).   The phase diagram with two massless and one massive quark flavors, $m_u = m_d = 0$ and $\Sigma m_s = 0.14$. Notations are the same with Fig. 1. In the narrow slit between the symmetric phase and the CFL phase, which can be seen in the right panel, only Δ_s has a large value.

have the same global structure, or topology, of the phases. It suggests that the qualitative structure of the phase diagram is not sensitive to the selection of the temperature-dependence schemes, as long as they hold the symmetry.

We next present the resulting phase diagram. Similar to the case with three equal-mass flavors, we need numerical calculations to evaluate the whole phase diagram. The result with $m = 0$ and $m_s \neq 0$ is shown in Fig. 2. At a small chemical potential, the diquark condensates do not have finite values in the ground state, and the phase diagram is the same with the model without the diquark condensates. Because for the ud quark flavors, there are no symmetry-breaking mass terms, the second-order phase transition line, as well as the TCP, exist. On the contrary, for the strange quark flavor, finite m_s breaks the chiral symmetry explicitly, and then the second-order phase transition line becomes a crossover. The TCP also becomes a critical point. In the symmetric phase, ϕ, Δ and Δ_s become exactly zero, but ϕ_s never becomes zero due to the finite symmetry-breaking term m_s.

As μ is increased with T kept small, a first-order phase transition to the 2SC phase is first observed. In the 2SC phase, not only Δ, but also ϕ_s, have large values. If μ is further increased, we next observe a phase transition to the CFL phase, where both Δ and Δ_s have large values. Note that because the flavor symmetry is explicitly broken, generally $\Delta \neq \Delta_s$ in the CFL phase. The diquark condensates become zero continuously when T and μ are increased. As seen in the right panel of Fig. 2, there is a narrow slit between two second-order phase transition lines for Δ and Δ_s. In this area, only Δ_s has a large value. We also show in detail the region around the end points of two horizontal second-order phase transition lines for Δ and the vertical first-order phase transition lines for ϕ_s and Δ_s in Fig. 3. We find the first-order phase transition between CFL phase and the phase with finite ϕ_s. The second-order phase transition line for Δ_s touches the first-order phase transition line for ϕ_s.

The result of the phase diagram can be considered as a function of m_s as follows; the 2SC phase appears as soon as m_s is turned on, and it extends as the symmetry-breaking parameter m_s is increased. In the model with anomaly effects [21,24–27], the flavor-mixing terms generally

make the phase diagrams robust under the small changes of the parameters. In our model, on the contrary, the anomaly effect is neglected, and the small symmetry breaking of m_s suddenly changes the phase diagram.

We consider the sequence of the melting of the diquark condensates. In the CFL phase, as T is increased with μ fixed, we find that the Δ becomes zero first, and the Δ_s becomes secondary. In the analysis of the NJL models [28,29], on the contrary, it was found that Δ_s melts first and Δ second, and then the phase with only Δ_s finite is not found. The 2SC phase (where only Δ is finite) above the CFL phase may also be expected in QCD. The reason is explained as follows [4,29]: Around the melting temperature, the quark Fermi spheres are smeared, and then the sizes of gaps are mainly dominated by the density of states. Because the larger m_s makes the strange quark Fermi sphere smaller, its density of states is smaller than that of the ud quarks, which results in the smaller Δ_s than Δ. This indicates the preceding melting of Δ_s. We consider that the contradicting result of our model is due to the absence of the Fermi sphere in our treatment and, unfortunately, that this is a limitation of our model.
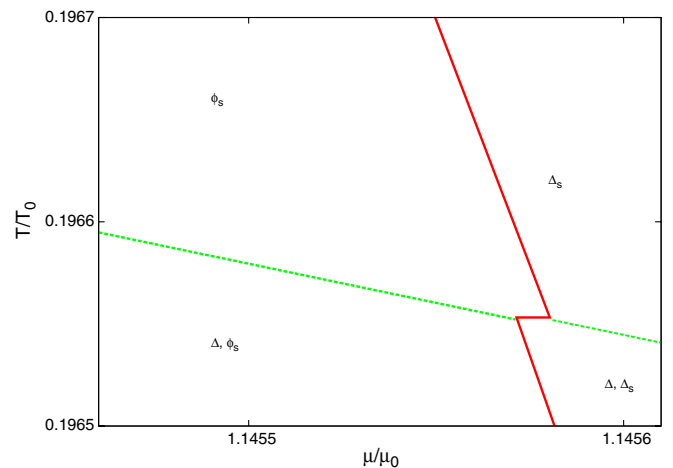

FIG. 3 (color online).   The phase diagram with two massless and one massive quark flavors, $m_u = m_d = 0$ and $\Sigma m_s = 0.14$. Notations are the same with Fig. 2.

VI. SUMMARY AND DISCUSSION

We have studied a ChRM model which can treat the competition between the chiral and the diquark condensates in the case with three flavors to investigate the phase diagram with the CFL phase. In order to describe the color superconductivity, we have introduced the color and Lorentz indices to the truncated Dirac matrix. The random matrices mimicking the gauge fields are taken to be real matrices, whose elements are distributed according to the Gaussian weight. After the integration over the random matrices, we are left with the four-fermion interaction term, which contains not only quark-antiquark interaction vertices, but also quark-quark vertices. Using Fierz transformations, the ratio of the coefficients is uniquely determined. Applying the bosonization techniques, we finally derive the effective potential as the function of the order parameters, the chiral condensates, and the diquark condensates.

The phase diagram on the $T - \mu$ plane is calculated by solving the gap equations simultaneously. In the case with three equal-mass quark flavors, we find the CFL phase in the large chemical potential region, while the chirally broken phase in the small chemical potential region. In the region where the CFL condensate is zero; the phase diagram is equivalent to that obtained from the conventional ChRM model without the diquark condensations. The CFL condensates become zero continuously, as T and/or μ are increased. The unphysical phase transition at large μ may be considered as the result of the fact that the ChRM model does not contain the Fermi surface. When finite quark mass m is introduced, the phase transition line for the CFL phase moves towards the larger chemical potential region. We also find that the region of the CFL phase becomes smaller as m is increased.

For the case with $2 + 1$ flavors, $m_u = m_d = 0$ and $m_s \neq 0$, we find both the CFL and the 2SC phases. Moreover, we find the phase where Δ_s has a finite value and $\Delta = 0$. Such a phase is not found in the NJL model, and not expected in QCD. We also consider that this phase may be a model artifact due to the absence of the Fermi surface, but cannot be excluded from the viewpoint of the symmetry.

Although there are unphysical points, the ChRM model studied in this paper can consistently address both the chirally broken phase and the CFL phase. In addition, with the finite asymmetry between the ud quarks and the strange quark, the model also can show the 2SC phase. Because the ChRM model includes the Dirac matrix, investigation of its eigenvalue distribution, the Dirac spectrum, may be possible. It may be possible to understand the phase transition into the diquark-condensed states in the context of the moving of the Dirac eigenvalues. Furthermore, in the microscopic region, there might be the universal structure of the Dirac spectrum, which can be compared to the other models at high density [30,31]. The applications in these directions are postponed to future studies.

Finally, we consider an outlook or a possible extension of the model. One of the most important effect we neglect is the $U(1)$ breaking axial anomaly effect. It is known that, in the ChRM model, the anomaly effect introduces the flavor mixing, which changes the phase diagram drastically [21,24,25]. Indeed, we find that the effective potential in the case with $2 + 1$ flavors and $\Delta_s = 0$ can be separated to the ud quark sector and the strange quark sector, as a result of the absence of the mixing effect. Moreover, on the phase diagram around mid-chemical potential, it is suggested that the anomaly effect, which also mixes the chiral and the diquark order parameters, plays a crucial role on the phase structure with the various superconducting phases [26,27,32]. We are then interested in combining the treatment of the ChRM model with the color-superconducting phases presented here, and of the ChRM model with the axial anomaly in Ref. [21] to investigate the effects of the axial anomaly on the phase structure with the color-superconducting phases. It will allow us to discuss the phase structure at finite temperature and density from a viewpoint of the symmetry.

[1] M. G. Alford, K. Rajagopal, and F. Wilczek, Nucl. Phys. **B537,** 443 (1999).

[2] M. G. Alford, J. Berges, and K. Rajagopal, Nucl. Phys. **B558,** 219 (1999).

[3] K. Rajagopal and F. Wilczek, *At the Frontier of Particle Physics*, edited by M. Shifman (World Scientific, Singapore, 2001), Vol. 3, p. 2061.

[4] K. Fukushima and T. Hatsuda, Rep. Prog. Phys. **74,** 014001 (2011).

[5] For a recent review, M. G. Alford, A. Schmitt, K. Rajagopal, and T. Schafer, Rev. Mod. Phys. **80,** 1455 (2008).

[6] T. Hatsuda and T. Kunihiro, Phys. Rep. **247,** 221 (1994).

[7] M. Buballa, Phys. Rep. **407,** 205 (2005).

[8] For a recent review, see C. DeTar, in Proceedings of the Kyoto workshop on Thermal Quantum Field Theory and its Application, Kyoto, Japan, 2010; arXiv:1101.0208.

[9] For a recent review, see P. de Forcrand, Proc. Sci., LAT2009 (2009) 010.

[10] B. C. Barrois, Nucl. Phys. **B129**, 390 (1977).

[11] D. Bailin and A. Love, Phys. Rep. **107**, 325 (1984).

[12] E. V. Shuryak and J. J. M. Verbaarschot, Nucl. Phys. **A560**, 306 (1993); A. D. Jackson and J. J. M. Verbaarschot, Phys. Rev. D **53**, 7223 (1996); T. Wettig, A. Schäfer, and H. A. Weidenmüller, Phys. Lett. B **367**, 28 (1996); **374**, 362(E) (1996); for review, J. J. M. Verbaarschot and T. Wettig, Annu. Rev. Nucl. Part. Sci. **50**, 343 (2000).

[13] A. M. Halasz, A. D. Jackson, R. E. Shrock, M. A. Stephanov, and J. J. M. Verbaarschot, Phys. Rev. D **58**, 096007 (1998).

[14] M. Asakawa and K. Yazaki, Nucl. Phys. **A504**, 668 (1989).

[15] A. Barducci, R. Casalbuoni, S. De Curtis, R. Gatto, and G. Pettini, Phys. Lett. B **231**, 463 (1989).

[16] B. Vanderheyden and A. D. Jackson, Phys. Rev. D **61**, 076004 (2000); **62**, 094010 (2000).

[17] B. Vanderheyden and A. D. Jackson, Phys. Rev. D **64**, 074016 (2001).

[18] B. Klein, D. Toublan, and J. J. M. Verbaarschot, Phys. Rev. D **72**, 015007 (2005).

[19] T. Banks and A. Casher, Nucl. Phys. **B169**, 103 (1980).

[20] K. Fukushima, J. High Energy Phys. 07 (2008) 083.

[21] T. Sano, H. Fujii, and M. Ohtani, Phys. Rev. D **80**, 034007 (2009).

[22] R. A. Janik, M. A. Nowak, G. Papp, and I. Zahed, Nucl. Phys. **B498**, 313 (1997).

[23] B. Vanderheyden and A. D. Jackson, Phys. Rev. D **72**, 016003 (2005).

[24] H. Fujii and T. Sano, Phys. Rev. D **81**, 037502 (2010).

[25] H. Fujii T. Sano Phys. Rev. D **83**, 014005 (2011).

[26] T. Hatsuda, M. Tachibana, N. Yamamoto, and G. Baym, Phys. Rev. Lett. **97**, 122001 (2006).

[27] H. Abuki, G. Baym, T. Hatsuda, and N. Yamamoto, Phys. Rev. D **81**, 125010 (2010).

[28] M. Buballa and M. Oertel, Nucl. Phys. **A703**, 770 (2002).

[29] K. Fukushima, C. Kouvaris, and K. Rajagopal, Phys. Rev. D **71**, 034002 (2005).

[30] N. Yamamoto and T. Kanazawa, Phys. Rev. Lett. **103**, 032001 (2009).

[31] G. Akemann, Int. J. Mod. Phys. A **22**, 1077 (2007).

[32] H. Basler and M. Buballa, Phys. Rev. D **82**, 094004 (2010).